Surface Sensitive Studies of the Reactive Uptake of Chlorine Nitrate on Ice

B. S. Berland, M. A. Tolbert, and S. M. George*

Department of Chemistry and Biochemistry and CIRES, University of Colorado, Boulder, Colorado 80309

Received: March 31, 1997; In Final Form: October 3, 1997[⊗]

The reactive uptake of chlorine nitrate ($ClONO_2$) on ice surfaces ($ClONO_2 + H_2O \rightarrow HOCl + HNO_3$) was studied with surface sensitivity using laser-induced thermal desorption (LITD) techniques. Thin films of vapor-deposited ice were exposed to $ClONO_2$ vapor at substrate temperatures from 75 to 140 K. The reactive uptake of $ClONO_2$ was directly measured by monitoring the hydrolysis reaction products, HOCl and HNO_3, on the ice surface in real time. At low temperatures from 75 to 110 K, the HOCl coverage initially increased rapidly with $ClONO_2$ exposure, indicating an efficient hydrolysis reaction. After longer $ClONO_2$ exposures, the rate of HOCl production decreased and the HOCl reached a constant coverage. A reaction probability of $\gamma = 0.03$ was calculated for the reactive uptake of $ClONO_2$ on ice and was independent of temperature from 75 to 110 K. At temperatures greater than 110 K, the reaction probability decreased with increasing temperature and reached a value of $\gamma = 0.005$ at 140 K. This decrease in the reaction probability with increasing substrate temperature is consistent with a precursor-mediated adsorption model. The good fits to the precursor-mediated adsorption model indicate that the $ClONO_2$ hydrolysis reaction has a low activation barrier. The precursor-mediated adsorption model extrapolated to stratospheric temperatures predicts a reaction probability that is significantly lower than the accepted literature value of $\gamma \sim 0.3$. This discrepancy may be caused by the higher pressures and the dynamic ice surface at stratospheric conditions that could enhance the reaction probability. The constant HOCl coverage reached after longer $ClONO_2$ exposures is attributed to the poisoning of the ice surface by product HNO_3. Calibrated HNO_3 signals at 86 and 140 K revealed that the $ClONO_2$ hydrolysis reaction is inhibited at a nitric acid coverage of $\sim 7.5 \times 10^{14}$ molecules/cm^2 or $\sim$ 1 monolayer. This coverage suggests that the hydrolysis reaction is limited to the surface or near-surface region of ice at these low temperatures.

I. Introduction

The hydrolysis of $ClONO_2$ has been extensively studied on several surfaces representative of stratospheric particulate.[1−9] The reaction probability, γ, has been measured to be $\gamma = 0.3$ on ice surfaces and $\gamma = 0.001$ on nitric acid-ice films at typical stratospheric temperatures of ~190 K.[10,11] The reaction products on ice under stratospheric conditions are HOCl that is released to the gas phase and HNO_3 that remains in the ice.[12,13] The HOCl may also react heterogeneously with HCl on polar stratospheric clouds (PSCs) to produce Cl_2. Photolysis of either HOCl or Cl_2 leads to Cl radicals that can efficiently destroy ozone. In addition, the HNO_3 that is sequestered on the PSCs prevents the reformation of the $ClONO_2$ reservoir and prolongs the lifetime of ClO radicals.

Although known to be important, a detailed reaction mechanism for heterogeneous chlorine nitrate hydrolysis is still lacking. An early proposal suggested an acid-catalyzed surface reaction that would lead to cleavage of the ClO−NO_2 bond.[14−17] However, more recent isotopic studies show that the Cl−ONO_2 bond is broken during $ClONO_2$ hydrolysis on ice surfaces.[2] In addition, several groups have reported that the reaction probability for $ClONO_2$ hydrolysis on a wide variety of substrates depends only on the H_2O activity.[1,5,18−20] The reaction mechanism has also been suggested to be a S_N2 nucleophilic attack by H_2O on the Cl in $ClONO_2$.[2,4,21,22] This mechanism would break the Cl−O bond and form products that are consistent with the isotopic studies.

In the present paper, the hydrolysis of chlorine nitrate on ice surfaces was studied with surface sensitive techniques. Thin films of vapor-deposited ice were exposed to $ClONO_2$ vapor at ice temperatures ranging from 75 to 140 K. The reactive uptake of $ClONO_2$ was directly measured by monitoring the hydrolysis reaction products, HOCl and HNO_3, on the ice surface in real time using laser-induced thermal desorption (LITD) techniques. The reactant and product surface stabilities were also investigated with temperature-programmed laser-induced thermal desorption (TP-LITD). These LITD studies determined the reaction probabilities for $ClONO_2$ on ice, and the temperature-dependent behavior revealed information about the hydrolysis activation barrier. Extrapolation of these reaction probabilities to stratospheric temperatures also allowed comparisons that indicate the possible importance of higher pressures and the dynamic ice surface at stratospheric conditions.

II. Experimental Section

A. Vacuum Chamber and Al_2O_3 Substrate. The experimental apparatus used for these studies has been described previously and is shown is Figure 1.[23,24] Briefly, a single-crystal Al_2O_3 (0001) substrate was mounted at the base of a liquid nitrogen cooled cryostat in an ultrahigh vacuum (UHV) chamber. The UHV chamber was pumped by a corrosive-resistant turbomolecular pump to a base pressure of $\sim 5 \times 10^{-9}$ Torr. Pressures were monitored with an ionization gauge. The chamber was also equipped with a mass spectrometer (UTI 100C) for laser desorption studies and residual gas analysis.

The back side of the Al_2O_3 substrate was coated with ~2000 Å of chromium to allow resistive heating of the substrate. The liquid nitrogen cooling in conjunction with resistive heating could obtain a wide range of temperatures from 86 to 500 K. Temperatures as low as 75 K could be attained by pumping on the liquid nitrogen reservoir with a mechanical pump. The

[⊗] Abstract published in *Advance ACS Abstracts,* November 15, 1997.

S1089-5639(97)01121-3 CCC: $14.00

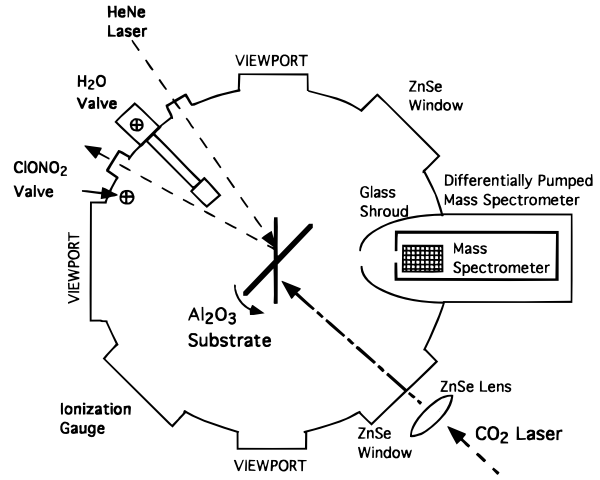

Figure 1. Experimental apparatus for the laser-induced thermal desorption (LITD) experiments of the reactive uptake of $ClONO_2$ on ice films. The ice films were grown on Al_2O_3 substrates.

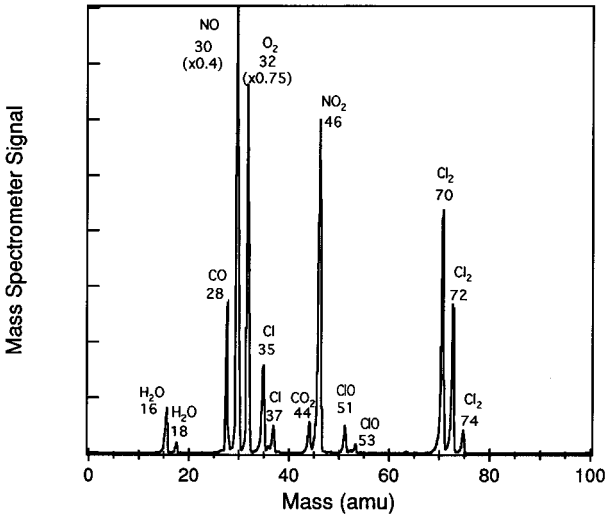

Figure 2. Typical mass spectrometer cracking pattern for gas-phase $ClONO_2$ at $P \approx 1 \times 10^{-6}$ Torr.

temperature was monitored with a type K thermocouple attached to the front face of the Al_2O_3 substrate using a ceramic adhesive (Aremco).

B. $ClONO_2$ Synthesis and Film Preparation. The $ClONO_2$ was prepared by reacting Cl_2O with N_2O_5 as described in the literature.[25] The $ClONO_2$ sample was vacuum distilled three times before use. Ultraviolet absorption analysis revealed that the vapor above the reservoir contained mostly pure $ClONO_2$. However, there were small Cl_2 (~10%) and Cl_2O (<5%) impurities. The $ClONO_2$ reservoir was held at −75 °C in a dry ice/ethanol bath. The $ClONO_2$ vapor above the reservoir was transferred to the UHV chamber using a glass gas line and introduced into the UHV chamber through a controlled leak valve.

A typical mass spectrometer trace for $ClONO_2$ ($P \sim 1 \times 10^{-6}$ Torr) is shown in Figure 2. The observed cracking pattern agrees well with the cracking pattern reported in the literature.[12] Figure 2 shows the characteristic peaks for ClO ($m/e = 51$ and 53), NO_2 ($m/e = 46$), and NO ($m/e = 30$). A peak was also observed at $m/e = 32$ and is probably a crack of NO_3 from $ClONO_2$ that produces O_2. The peak at $m/e = 32$ is observed for both $ClONO_2$ and HNO_3, and the peak magnitude scales with the gas pressure. The magnitude of $m/e = 32$ relative to $m/e = 28$ is too large for the signal to be O_2 from a leak. The other masses in the cracking pattern are impurities that enter the chamber with the $ClONO_2$. Masses $m/e = 35$, 37, 70, 72, and 74 are from the Cl_2 impurity. The mass spectrum also shows H_2O ($m/e = 18$) that is present in a UHV background, and CO ($m/e = 28$) and CO_2 ($m/e = 44$) are background gases in the gas line.

Purging the chamber was necessary to achieve the cracking pattern shown in Figure 2. The $ClONO_2$ initially decomposed on the metal walls, and no signal was observed at $m/e = 51$ and $m/e = 53$. As the $m/e = 51$ and $m/e = 53$ signals initially appeared, a significant amount of HOCl was also observed at $m/e = 52$ and $m/e = 54$. The chamber was purged until the cracking pattern showed ClO with no HOCl. Once the system was passivated, a ~15 min daily purge was sufficient to achieve this cracking pattern for the remainder of the day.

After the system was passivated, $ClONO_2$ films were condensed onto the cooled Al_2O_3 substrate or ice surfaces. $ClONO_2$ pressures were typically in the 10^{-7} Torr range. $ClONO_2$ multilayers were stable at $T < 110$ K on both the ice and Al_2O_3 surfaces. An LITD survey of the masses in a pure $ClONO_2$ multilayer revealed primarily LITD signals corresponding to ClO ($m/e = 51$), NO ($m/e = 30$), and NO_2 ($m/e = 46$) that are consistent with a pure $ClONO_2$ film. Small LITD signals were also observed for Cl_2 and H_2O. In addition, there were small LITD signals corresponding to HOCl and HNO_3 that were present in H_2O multilayers prior to $ClONO_2$ exposure. HOCl and HNO_3 presumably formed by heterogeneous reaction of H_2O with $ClONO_2$ on the liquid nitrogen cryostat or chamber walls.

Pure ice films for the reaction studies and pure HNO_3 films for mass spectrometer calibrations were prepared by vapor deposition onto the cooled Al_2O_3 substrate. The H_2O and HNO_3 reservoirs were prepared as described previously.[23] The H_2O and HNO_3 vapors were introduced into the chamber through leak valves with dosing heads. All ice films were prepared at $T = 140$ K and $P_{H_2O} \approx 1 \times 10^{-6}$ Torr. Past studies have shown ice films prepared under these conditions will form dense ice.[26] These conditions were chosen to avoid complications from microporous ice that can form at colder temperatures and higher H_2O partial pressures.[26]

C. Optical Interference Techniques. Optical interference techniques were used to monitor the film thickness.[23] A HeNe laser ($\lambda = 6328$ Å) was reflected from the growing films at near normal incidence as shown in Figure 1. The reflectance was monitored with a Hamamatsu R928 photomultiplier tube. The Al_2O_3 substrate was slightly wedged to allow for separation of the reflections from the front and back faces. The film thickness, x, can then be calculated from eq 1

$$x = \frac{m\lambda}{2n(T)\cos\phi} \tag{1}$$

where $n(T)$ is the temperature-dependent refractive index, ϕ is the angle of refraction, and m is the number of periods of oscillation.

Optical interference techniques can also be used to measure the film thickness of multilayered film systems or for noninteger periods of oscillation.[27,28] However, the reflectance does not change dramatically for film thicknesses, $x < 100-200$ Å. The uncertainty of the optical interference measurements is much greater for these thin films. The refractive indices are $n = 1.76$ for Al_2O_3,[29] $n = 1.31$ for ice,[26] and $n = 1.46$ for HNO_3.[23,30] The real refractive index can also be measured with optical interference techniques.[23] The present experiments measured a refractive index of $n = 1.48 \pm 0.02$ for $ClONO_2$ multilayers deposited at 90 K.

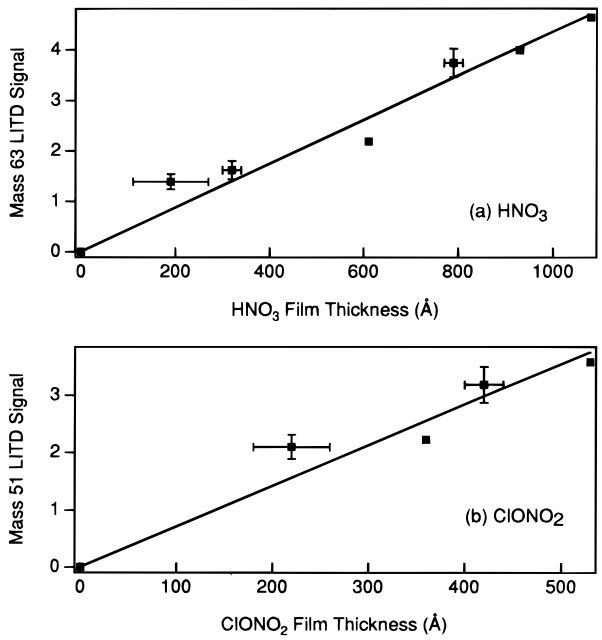

Figure 3. Calibration of the LITD signals for a) HNO_3 at $m/e = 63$ and (b) $ClONO_2$ at $m/e = 51$. The film thicknesses were determined using optical interference techniques. Error bars are indicated for representative points. The solid lines represent a linear least-squares fit to the data.

D. Laser-Induced Thermal Desorption (LITD). The LITD techniques have been described in detail previously.[23] In short, a Lumonics pulsed TEM-00 CO_2 TEA laser at $\lambda = 10.6$ μm was used for these LITD measurements. The resultant CO_2 laser beam had a Gaussian spatial distribution, a pulse duration of ~100 ns (fwhm), and an energy of ~70 mJ/pulse.[31] The CO_2 laser beam was focused onto the Al_2O_3(0001) surface at 45° relative to the surface normal using an $f = 75$ cm focal length ZnSe lens. The focused laser beam illuminated an elliptical area approximately 0.75 mm × 1.1 mm on the Al_2O_3 surface.

The incident CO_2 laser radiation was absorbed by the adsorbed layer and the Al_2O_3(0001) substrate leading to a rapid localized heating of the illuminated area. This rapid heating induced the desorption of the adsorbed layer. The crystal positioning allowed the desorption burst to travel directly to the ionizer of the quadrupole mass spectrometer for line-of-sight detection. The mass spectrometer was isolated from the chamber by a glass shroud.[32] The mass spectrometer was also differentially pumped using a liquid nitrogen cooled copper cylinder that encased the mass spectrometer.[32] Monolayer and submonolayer adsorbate coverages could be detected with this line-of-sight detection and differential pumping. The ~1 mm elliptical desorption area allowed the surface coverage to be monitored at 15 individual locations across the crystal. One CO_2 laser pulse desorbed >90% of the adsorbed layer in each desorption area. The H_2O LITD signals were reproducible to ±10% for various ice multilayers on the Al_2O_3 substrate.

The desorbed gases were monitored with a UTI 100C quadrupole mass spectrometer. The parent signals from HOCl ($m/e = 52$) and HNO_3 ($m/e = 63$) were the only unique masses that could be used to monitor the $ClONO_2$ hydrolysis reaction. For HNO_3 and $ClONO_2$, the LITD signals were calibrated using pure multilayers of known thickness that were characterized using optical interference techniques. Figure 3a shows that the $m/e = 63$ HNO_3 LITD signal is linear with HNO_3 film thickness. The HNO_3 film thickness can be converted to a coverage in molecules/cm^2 using the density of $\rho = 1.88$ g/cm^3 for solid HNO_3.[33] A two-point calibration of HNO_3 was performed daily to check for drift in the mass spectrometer sensitivity. The HOCl could not be directly calibrated because a pure source of HOCl was not readily available. An indirect calibration of the HOCl signals using HNO_3 was performed and is discussed in section III.A.

ClO at $m/e = 51$ and NO_2 at $m/e = 46$ were monitored to measure $ClONO_2$. Figure 3b shows that the ClO signal at $m/e = 51$ is linear with film thickness for pure $ClONO_2$ films. The $ClONO_2$ film thicknesses were determined by optical interference techniques. Although the LITD signal at $m/e = 51$ is linear with $ClONO_2$ film thickness for pure $ClONO_2$ films, ClO at $m/e = 51$ is also a crack of HOCl. Similarly, the LITD signal at $m/e = 46$ for $ClONO_2$ is also a major crack of HNO_3. Consequently, $ClONO_2$ did not have a unique mass that could unambiguously identify $ClONO_2$ in the presence of HOCl and HNO_3.

III. Results

A. Reactive Uptake of $ClONO_2$ on Ice at 86 K. The reactive uptake of $ClONO_2$ on ice at 86 K was studied by directly monitoring the hydrolysis reaction products HOCl and HNO_3 in real time using laser-induced thermal desorption (LITD) techniques. The HOCl LITD signals were larger and more consistent than the HNO_3 LITD signals. Consequently, the reactive uptake of $ClONO_2$ on ice was monitored primarily with HOCl LITD signals. The reactive uptake of $ClONO_2$ was also measured using the HNO_3 LITD signals to confirm the HOCl results.

To study the reactive uptake of $ClONO_2$ on ice at 86 K, a ~150 Å thick ice film was first deposited on the Al_2O_3 substrate at 140 K to form a dense ice multilayer.[26] The substrate temperature was then lowered to 86 K, and the Al_2O_3 substrate was positioned to face the mass spectrometer. Subsequently, HOCl LITD signals were recorded to determine the background HOCl coverage prior to $ClONO_2$ exposure. The $ClONO_2$ valve was then opened to obtain a pressure of 5×10^{-7} Torr and the HOCl LITD signal at $m/e = 52$ was monitored as a function of time.

The HOCl coverage as a function of $ClONO_2$ exposure for a typical experiment is shown by the open squares in Figure 4. Each point represents a separate desorption area on the Al_2O_3 crystal. There was some scattering in the HOCl LITD signals. Consequently, the HOCl LITD signals between the first two and last two LITD signals have been smoothed using an averaging routine, $\bar{x}_n = (x_{n-2} + x_{n-1} + x_n + x_{n+1} + x_{n+2})/5$, where n represents the nth point in the data array.

The first open square shows that there was a small amount of HOCl in the ice film prior to the opening of the $ClONO_2$ valve. The origin of the initial HOCl LITD signal at $m/e = 52$ is presumably the reaction of H_2O with $ClONO_2$ on the liquid nitrogen cryostat or chamber walls during the formation of the ice films. This initial background HOCl LITD signal is only ~15% of the HOCl LITD signal after long $ClONO_2$ exposures. In addition, the background HOCl should be evenly spread throughout the ice film. Consequently, the background HOCl on the ice surface prior to $ClONO_2$ exposure should be minimal and should not have a significant effect on the $ClONO_2$ hydrolysis reaction.

In addition to the small amount of HOCl in the ice film prior to $ClONO_2$ exposure, HOCl may be deposited on the ice film during the $ClONO_2$ exposure due to impurities or reaction on the chamber walls. The open triangles in Figure 4 show an estimate for the amount of HOCl that could be deposited as a result of wall reactions or impurities during the $ClONO_2$ exposure. To obtain this estimate, a ~150 Å ice film was

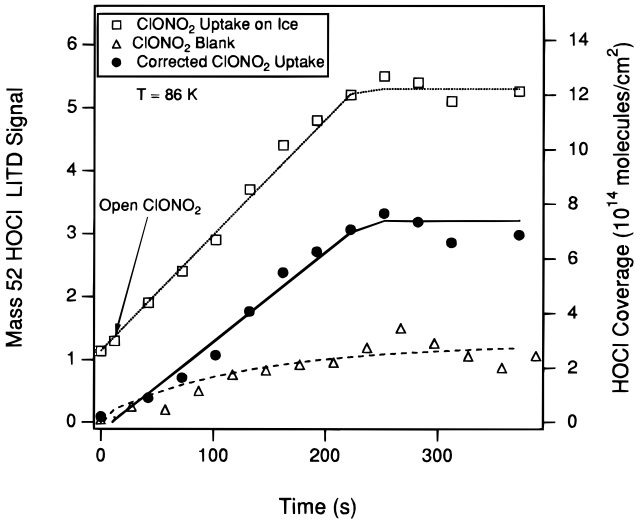

Figure 4. Reactive uptake of $ClONO_2$ on ice at 86 K and $P_{ClONO_2} = 5 \times 10^{-7}$ Torr as monitored by the HOCl LITD signal at $m/e = 52$. The open squares and solid circles represent the uncorrected and corrected HOCl LITD signals, respectively. The lines associated with these signals were determined from a linear regression analysis. The open triangles show the HOCl LITD signals from the blank experiment. The HOCl LITD signals shown on the right-hand axis were calibrated using HNO_3.

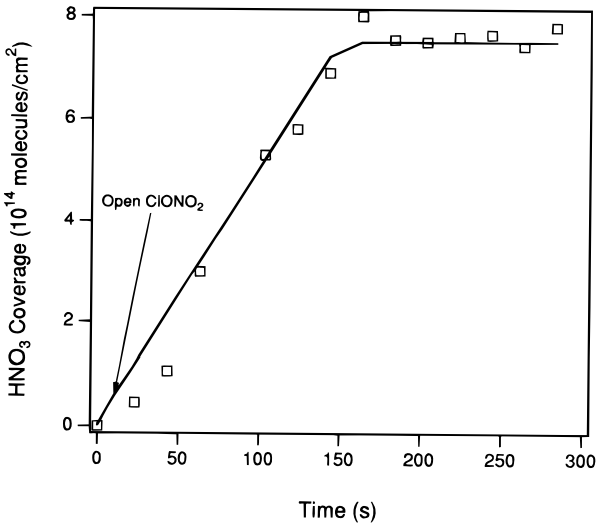

Figure 5. Reactive uptake of $ClONO_2$ on ice at 86 K and $P_{ClONO_2} = 1 \times 10^{-6}$ Torr as monitored by the HNO_3 LITD signals at $m/e = 63$. The solid line was generated from linear least squares data analysis.

initially prepared at 140 K to form a dense ice multilayer. The substrate temperature was then raised to 180 K to completely desorb the ice film.[24] The substrate temperature was then lowered back to 86 K, and the $ClONO_2$ valve was opened to obtain a pressure of 5×10^{-7} Torr. The HOCl LITD signals from the Al_2O_3 surface during this blank experiment were then monitored versus time.

The HOCl coverage that is monitored without the ice film is much smaller than the increase in HOCl coverage that is measured on the ice film versus $ClONO_2$ exposure. This blank experiment reveals that only a minimal amount of HOCl is produced by processes other than $ClONO_2$ hydrolysis reaction on the ice film. The solid circles represent the HOCl coverage that has been corrected for the initial background HOCl and the blank experiment. The corrected HOCl coverage initially increases rapidly indicating that the $ClONO_2$ hydrolysis reaction is efficient even at 86 K.

The apparent saturation of the HOCl coverage in Figure 4 at $t \approx 200$ s is attributed to the poisoning of the ice surface by product HNO_3. The reaction probability for $ClONO_2$ hydrolysis on nitric acid-ice at stratospheric temperatures is a factor of 300 smaller than the reaction probability obtained on ice.[11] Previous studies under stratospheric conditions also indicate that nitric acid poisoning of the ice surfaces can be rapid.[10] Similar effects would be expected at the lower temperatures of the present experiments. If the ice surface is converted to a nitric acid-ice surface in ~200 s and the reaction probability decreased by ×300, the HOCl LITD signals shown in Figure 4 would only increase from ~5.5 to 5.6 for the time period from $t =$ 200 to $t = 350$ s. This small change in the HOCl LITD signal would be well within the typical scatter of the LITD measurements, and the HOCl coverage would appear constant with time.

Figure 5 shows the reactive uptake of $ClONO_2$ on the ice film at 86 K as monitored by the growth of the HNO_3 LITD signals. These HNO_3 LITD signals have also been smoothed using the averaging routine where this routine is applicable. The HNO_3 LITD signals were monitored during $ClONO_2$ exposure at a pressure of 1×10^{-6} Torr. The HNO_3 coverage displayed in Figure 5 has been corrected for the HNO_3 coverage of ~ 1.4×10^{15} molecules/cm^2 in the initial ice film. The initial HNO_3 coverages are large because the pumping speed for HNO_3 is very slow. Consequently, the background HNO_3 pressures are high, and they produce HNO_3 impurities in the initial ice film. The initial HNO_3 coverage of $\sim 1.4 \times 10^{15}$ molecules/cm^2 prior to the $ClONO_2$ exposure is presumably evenly distributed in the 150 Å ice film, and the ice film stoichiometry should be >25:1 H_2O:HNO_3.

Figure 5 shows that the HNO_3 coverage increases with $ClONO_2$ exposure until ~150 s. The HNO_3 LITD signals show that the $ClONO_2$ hydrolysis reaction saturates at a HNO_3 coverage of $\sim(7.5 \pm 2.3) \times 10^{14}$ molecules/cm^2. This HNO_3 coverage is approximately equivalent to the number of H_2O surface sites on the basal plane of hexagonal ice (1 monolayer = 1 ML = 1.15×10^{15} molecules/cm^2).[34] Since the ice films are ~50 monolayers thick, this HNO_3 coverage indicates that the $ClONO_2$ hydrolysis reaction is probably limited to the surface or near surface region of the ice film at 86 K.

The HNO_3 coverages produced by the hydrolysis reaction were also measured on thicker ice films with thicknesses up to ~500 Å. Unfortunately, the background HNO_3 levels were larger for the thicker ice films, and the HNO_3 LITD data was very scattered. The best fit to the data from these thicker films revealed a HNO_3 coverage that was in good agreement with the saturation HNO_3 coverage observed on the ~150 Å ice films.

The stoichiometry of the $ClONO_2$ hydrolysis reaction indicates that one $ClONO_2$ molecule reacts to form one HOCl molecule and one HNO_3 molecule. Past laboratory experiments at stratospheric temperatures have confirmed this stoichiometry.[9,13] Assuming the reaction is also stoichiometric at 86 K, the saturated HNO_3 and HOCl coverages are both $\sim 7.5 \times 10^{14}$ molecules/cm^2. The right-hand vertical axis of Figure 4 shows the calibrated HOCl coverage assuming that the saturated HOCl coverage is 7.5×10^{14} molecules/cm^2.

B. Reactive Uptake of $ClONO_2$ versus Ice Temperature. The reactive uptake of $ClONO_2$ was studied versus ice temperature from 75 to 140 K. Because of the background problems for HNO_3, the reactive uptake was measured primarily using HOCl LITD signals at the various ice temperatures. The HNO_3 LITD signals were also monitored versus $ClONO_2$ exposure at ice temperatures of 86 and 140 K. All of the ice films were initially prepared at 140 K to avoid the formation of microporous ice.[26] After adjusting the ice temperature, the $ClONO_2$ valve was opened to obtain a pressure of 5×10^{-7} Torr.

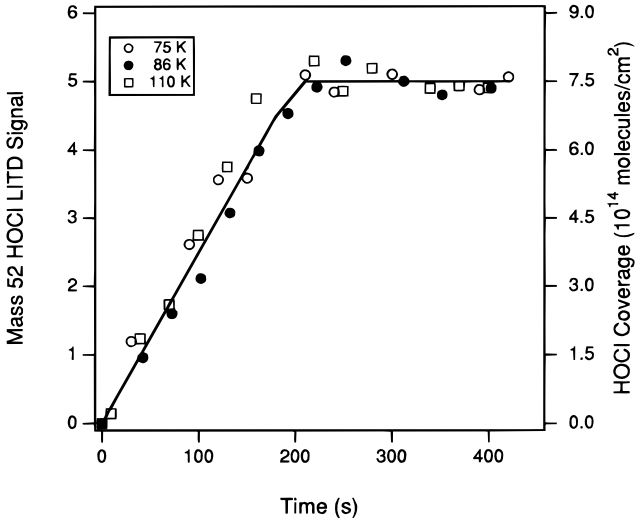

Figure 6. Temperature-independent reactive uptake of $ClONO_2$ on ice at $P_{ClONO_2} = 5 \times 10^{-7}$ Torr and low temperatures as monitored by the HOCl LITD signals at $m/e = 52$. All HOCl LITD signals have been corrected using the HOCl LITD signals from the blank. The solid lines represent a linear least-squares fit to the data.

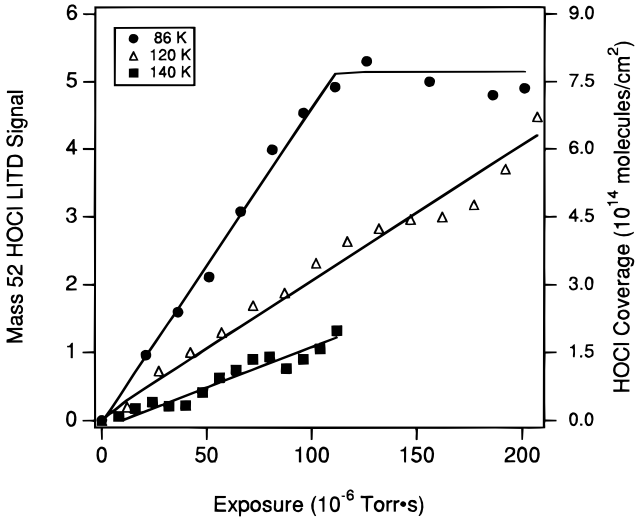

Figure 7. Temperature-dependent reactive uptake of $ClONO_2$ on ice at various temperatures as monitored by the HOCl LITD signals at $m/e = 52$. The solid lines represent a linear least-squares fit to the data.

Figure 6 shows the reactive uptake of $ClONO_2$ on ice at low temperatures, $T = 75-110$ K, as monitored by the HOCl LITD signals. The HOCl LITD signals have been smoothed and have also been corrected for the initial background HOCl coverage and the blank experiment. The right vertical axis shows the HOCl coverage assuming that the saturated HOCl coverage is 7.5×10^{14} molecules/cm^2 based on the HNO_3 calibration. Figure 6 shows that the rate of HOCl production and the rate of $ClONO_2$ hydrolysis is independent of temperature for $T \leq 110$ K.

The smoothed HOCl LITD signals as a function of $ClONO_2$ exposure for $T = 86$, 120, and 140 K are shown in Figure 7. These HOCl LITD signals are shown versus exposure because each experiment was performed at a slightly different $ClONO_2$ pressure. The rate of HOCl production on the ice film decreases with increasing temperature. This decrease is not the result of increased HOCl desorption at higher ice temperatures. Figure 8 shows the stability of HOCl on ice films at $T = 140$ K. An HOCl coverage of ~1 ML was deposited by reacting $ClONO_2$ on ice at 90 K. The temperature was then increased to 140 K,

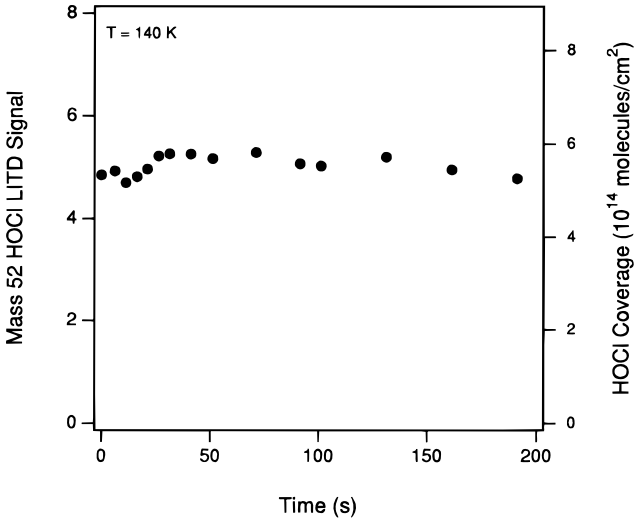

Figure 8. Stability of ~1 ML of HOCl on ice at $T = 140$ K.

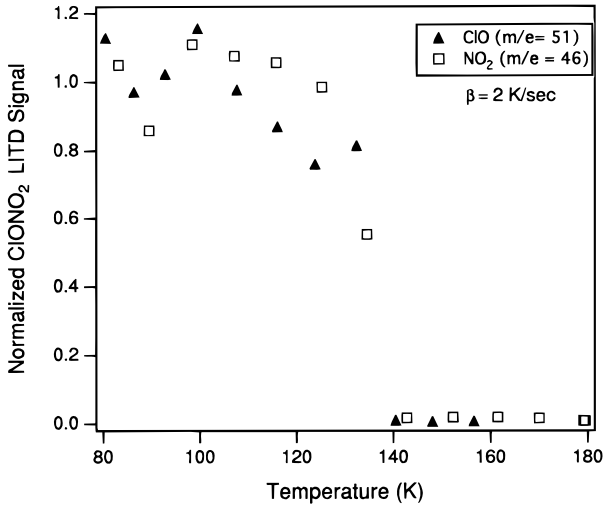

Figure 9. Temperature-programmed laser-induced thermal desorption (TP-LITD) results from a pure $ClONO_2$ multilayer. The heating rate was $\beta = 2$ K/s.

and the HOCl coverage was monitored versus time using the HOCl LITD signals. The smoothed HOCl signals shown in Figure 8 show no appreciable change in the HOCl coverage. Consequently, HOCl desorption is negligible on the time scale of the experiments shown in Figure 7.

The production of HNO_3 during $ClONO_2$ hydrolysis was measured at 86 and 140 K to corroborate the HOCl results. The results for HNO_3 were consistent with the HOCl results. The HNO_3 production rate at 140 K was slower than at 86 K. However, when the reaction was allowed to proceed to saturation at 140 K, the reaction saturated at a HNO_3 coverage of $\sim 7.5 \times 10^{14}$ molecules/cm^2. This saturation HNO_3 coverage is equal to the saturation HNO_3 coverage observed at 86 K. These HNO_3 results confirm that the $ClONO_2$ hydrolysis reaction is probably limited to the surface or near-surface region of the ice films at $T \leq 140$ K.

C. Thermal Stability of Reactants and Products. Temperature-programmed laser-induced thermal desorption (TP-LITD) experiments were used to measure the thermal stability of the $ClONO_2$ reactant and the HOCl and HNO_3 products. Figure 9 shows the LITD signals from $ClONO_2$ multilayers on the Al_2O_3 substrate as a function of substrate temperature. For these experiments, a $ClONO_2$ film with a thickness of ~150 Å was deposited at 75 K. The LITD signals for ClO at $m/e = 51$ or NO_2 at $m/e = 46$ were monitored every ~10 K while the

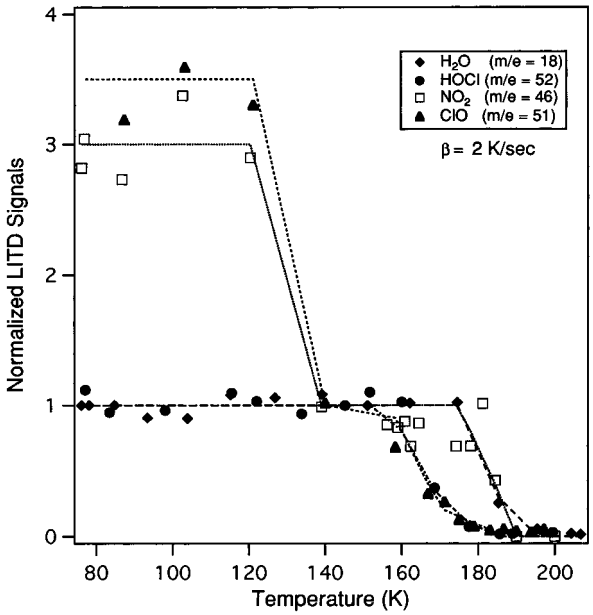

Figure 10. Temperature-programmed laser-induced thermal desorption (TP-LITD) results from a $ClONO_2$ multilayer on an ice multilayer. The heating rate was $\beta = 2$ K/s. The lines are intended for clarity in presentation.

substrate temperature was increased at a rate of $\beta = 2$ K/s. The ClO and NO_2 LITD signals were measured separately using two different $ClONO_2$ films with approximately the same thickness. The ClO and NO_2 LITD signals in Figure 9 have not been smoothed and have been normalized to their values at 75 K.

The ClO and NO_2 LITD signals in Figure 9 both reveal that the $ClONO_2$ multilayer is stable and $ClONO_2$ desorption is negligible at low temperatures, $T < 110$ K. The $ClONO_2$ desorption rate increases with increasing temperature above 110 K, and the LITD signals indicate that the $ClONO_2$ multilayer has completely desorbed by $T \sim 140$ K. Optical interference isothermal desorption measurements confirm that the $ClONO_2$ multilayer begins to desorb at $T \sim 110-120$ K.

TP-LITD experiments can also be utilized to monitor the reactants and products of the $ClONO_2$ hydrolysis reaction on an ice surface. In these experiments, a ~150 Å thick ice film was initially deposited at 140 K. A $ClONO_2$ multilayer with a thickness of ~20−50 Å was then deposited on the ice surface at 75 K. Subsequently, a TP-LITD experiment was performed at a heating rate of $\beta = 2$ K/s to monitor the $ClONO_2$, HOCl, HNO_3, and H_2O coverages. Each molecule was monitored in a separate TP-LITD experiment. The results from the various TP-LITD experiments are shown in Figure 10. These LITD signals have not been smoothed and have been normalized to their values at 140 K.

The ClO ($m/e = 51$) and NO_2 ($m/e = 46$) LITD signals show that a $ClONO_2$ multilayer initially exists on the ice multilayer. Figure 10 reveals that the $ClONO_2$ multilayer desorbs by 140 K. This behavior is expected based on the results shown in Figure 9. The NO_2 LITD signal that remains above 140 K is derived from HNO_3. The H_2O LITD signals in Figure 9 show that the ice multilayer begins to desorb at ~180 K and has completely desorbed by ~190 K. Previous studies have measured the zero-order H_2O desorption kinetics from ice.[24] The H_2O multilayer coverage versus temperature is in agreement with the coverage predicted by these desorption rates.

The NO_2 signal from HNO_3 scales with the H_2O LITD signal. Although the product HNO_3 is limited to the surface or near-surface region, ~60% of the HNO_3 signal is from background HNO_3 that should be evenly distributed in the ice film. This HNO_3 should decrease at approximately the same rate as the H_2O multilayer. The H_2O and HNO_3 LITD signals persist until ~190 K because the ice films have an initial thickness of ~150 Å. This H_2O coverage, the H_2O desorption kinetics, and the heating rate of $\beta = 2$ K/s together define the temperature required to desorb the entire ice film. H_2O LITD signals would be observed until even higher temperatures for thicker ice films.

The HOCl LITD signals are constant until ~160 K and then progressively decrease to zero. These HOCl TP-LITD results appear to show that the HOCl desorbs much earlier than the H_2O in the ice film. However, the H_2O will desorb from ice at a rate of ~1 ML/s at 160 K.[24] If the HOCl desorbs at the same rate as H_2O from ice and if the HOCl resides in the first five monolayers, the HOCl should all desorb by 170 K. The loss of 80% of the HOCl TP-LITD signal by 170 K confirms that the $ClONO_2$ hydrolysis reaction is confined to the surface or near-surface region of the ice film.

IV. Discussion

A. Reaction Probability for $ClONO_2$ Hydrolysis. The reaction probability, γ, is defined as the ratio of the number of collisions that lead to reaction divided by the total number of collisions with the surface. The total number of collisions with the surface can be calculated from the gas flux, $\phi = n\upsilon/4$, from gas kinetic theory. In this expression, n is the number density and υ is the average velocity of the gas molecules. For a $ClONO_2$ pressure of 5×10^{-7} Torr and a gas temperature of 298 K, the gas flux is $\phi = 1 \times 10^{14}$ collisions/cm^2 s.

The number of collisions that lead to reaction can be determined from the rate of appearance of reaction products. The rate of increase of the HOCl and HNO_3 product coverages are equivalent to the rate of reactive uptake of $ClONO_2$.[9,13] Linear regressions were performed on the data in Figures 4 and 5 to obtain the rate of HOCl and HNO_3 production. The regressions were all similar until the onset of the saturation coverage. The measured reaction probabilities were $\gamma = 0.031 \pm 0.005$ from the HOCl LITD signals and $\gamma = 0.024 \pm 0.01$ from the HNO_3 LITD signals. The uncertainty in the reaction probability represents the scatter on the LITD signals. These reaction probabilities agree within the experimental errors. Because of the large HNO_3 background, most of the reaction probabilities were obtained from HOCl LITD signals.

Linear regressions were performed at all temperatures, and the reaction probabilities versus temperature are shown in Figure 11. The reaction probability at 140 K was also studied versus $ClONO_2$ pressure from 1 to 8 x 10^{-7} Torr. The reaction probability of $\gamma = 0.005$ at 140 K was independent of pressure in this pressure range. The uncertainty in the reaction probabilities is dominated by the scatter of the LITD signals. These error bars are indicated in Figure 11. The absolute $ClONO_2$ pressure measured by the ionization gauge could also be in error by as much as a factor of 2.[35] This systematic error leads to an estimated uncertainty on the reaction probability at 86 K of $\gamma = 0.03$ (+0.03, −0.02). This reaction probability will be higher if the actual $ClONO_2$ pressure is only a fraction of the total pressure measured by the ionization gauge.

B. Precursor-Mediated Adsorption Model. Figure 11 shows the reaction probability for $ClONO_2$ hydrolysis on ice as a function of the ice temperature. The reaction probability is nearly independent of temperature from 75 to 110 K. At $T > 110$ K, there is a significant decrease in the reaction probability. This decrease in reaction probability with increasing temperature is consistent with a precursor-mediated adsorption model.[36,37]

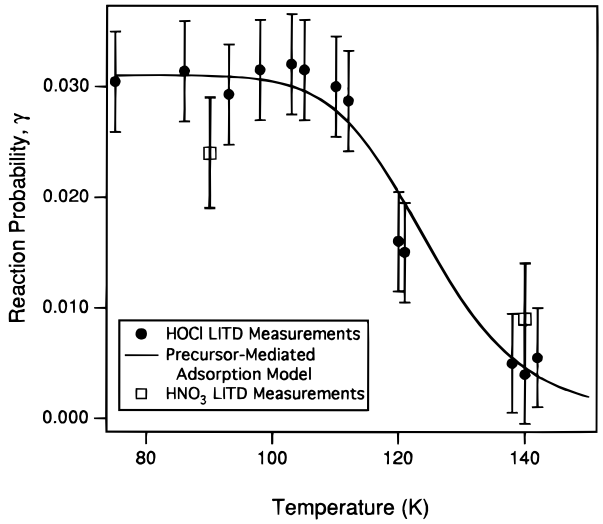

Figure 11. Reaction probability for $ClONO_2$ hydrolysis on ice as a function of ice temperature. The symbols represent the LITD measurements. The line represents the best fit using the precursor-mediated adsorption model.

The precursor model can be summarized by the following equations:

$$ClONO_2(g) \xrightarrow{\alpha\phi} ClONO_2(ad) \quad (2)$$

$$ClONO_2(ad) \xrightarrow{k_d} ClONO_2(g) \quad (3)$$

$$ClONO_2(ad) + H_2O \xrightarrow{k_r} HOCl(ad) + HNO_3(ad) \quad (4)$$

Equation 2 represents adsorption of a physisorbed $ClONO_2$ precursor onto the ice film. The rate of adsorption is given by $\alpha\phi$, where ϕ is the flux of $ClONO_2$ molecules onto the surface and α is the trapping probability. The physisorbed $ClONO_2$ precursor can then either desorb or react with H_2O on the ice surface. Equation 3 represents desorption with the rate constant, k_d. The reaction to form HOCl and HNO_3 with the reaction rate constant, k_r, is given by eq 4.

The steady-state approximation ($d\theta/dt \approx 0$) can be used to solve for θ_{ClONO_2}, the coverage of $ClONO_2$(ad). This $ClONO_2$ steady-state coverage can then be used to calculate the $ClONO_2$ hydrolysis reaction rate, $R = k_r\,\theta_{ClONO_2}$. The reaction probability, γ, is given by R/ϕ and is expressed by eq 5

$$\gamma = \frac{\alpha}{1 + \frac{k_d}{k_r}} \quad (5)$$

Because the trapping probability, α, is relatively independent of the substrate temperature,[36] the temperature dependence of eq 5 is contained in the k_d and k_r rate constants. For $T < 110$ K, the desorption rate is negligible and eq 5 simplifies to $\gamma = \alpha$. Consequently, the $ClONO_2$ hydrolysis reaction probability is constant at these low temperatures and Figure 11 shows that $\alpha = \gamma \approx 0.03$.

At higher temperatures, the desorption rate becomes significant and the precursor-mediated adsorption model predicts that γ should decrease with increasing temperature. This decrease in reaction probability reflects a lower surface residence time for the physisorbed $ClONO_2$ precursor. Assuming an Arrhenius temperature dependence for the rate constants for desorption and reaction, the temperature dependence of the reaction probability is

$$\gamma = \frac{\alpha}{1 + \frac{\nu_d}{\nu_r}\exp(-(E_d - E_r)/kT)} \quad (6)$$

The data for the reaction probabilities in Figure 11 were fit using eq 6. The best fit was achieved with $\nu_d/\nu_r = 10^7$ and $E_d - E_r = 4.1$ kcal/mol.

Theoretical calculations estimate that $E_d \sim 7$ kcal/mol.[38] Using this calculated value of E_d together with $E_d - E_r = 4.1$ kcal/mol, the precursor fit predicts a value of $E_r \approx 3$ kcal/mol. This value agrees well with previous estimates of ~3−7 kcal/mol.[21,39] In particular, a low activation barrier of $E_r \sim 3$ kcal/mol is consistent with recent theoretical ab initio calculations that show an efficient reaction with a low activation barrier of ~ 3 kcal/mol.[21] These calculations show that the lowest energy path for the $ClONO_2$ hydrolysis reaction is S_N2 nucleophilic attack by H_2O. This nucleophilic attack on the chlorine in $ClONO_2$ is facilitated by proton transfer from the attacking H_2O molecule to a neighboring H_2O molecule in the ice lattice. Assuming a typical desorption barrier of $\nu_d = 10^{13}$ s^{-1}, the ratio of preexponentials of $\nu_d/\nu_r = 10^7$ gives a reaction preexponential of $\nu_r = 10^6$ s^{-1}. This preexponential is low, but small preexponentials have been previously observed for surface reactions that proceed through a cyclic transition state.[40]

C. Comparison with Measurements at Stratospheric Temperatures. The reaction probability for $ClONO_2$ hydrolysis has been measured to be $\gamma \sim 0.3$ on ice at stratospheric conditions with $T \sim 190$ K.[11] The precursor-mediated reaction probabilities extrapolated to stratospheric temperatures are shown in Figure 12. At these temperatures, the precursor-mediated adsorption model given by eq 6 would predict $\gamma \approx 0.0001$. This extrapolated reaction probability is considerably lower than the actual measurements.

There are several possible explanations for this discrepancy. The high pressures under stratospheric conditions may enhance the $ClONO_2$ surface lifetime and lead to higher reaction probabilities. The larger stratospheric reaction probabilities could also be explained by a more dynamic ice surface. Another possible source of the discrepancy could be inaccurate assumptions regarding the ice surface area used in the stratospheric measurements. Alternatively, the low LITD reaction probabilities may be consistent with $ClONO_2$ hydrolysis on a partially HNO_3 poisoned ice surface or overestimated $ClONO_2$ pressures.

$ClONO_2$ molecules interacting with the ice surface at stratospheric pressures may experience multiple collisions with surrounding gas molecules that may enhance the reaction probability. Using a desorption activation barrier of ~7 kcal/mol[21] and assuming a typical desorption preexponential of 10^{13} s^{-1}, $ClONO_2$ has a predicted surface lifetime of $\tau_d \sim 10$ μs at 190 K. At typical stratospheric pressures of ~ 50 Torr,[11] there are ~200 collisions of primarily N_2 and O_2 molecules at every H_2O site on the ice surface in 10 μs. These collisions may help to trap the $ClONO_2$ on the ice surface and enhance its surface lifetime. This enhanced surface lifetime may significantly increase the $ClONO_2$ hydrolysis reaction probability.

The existence of a more dynamic ice surface at stratospheric conditions could also explain the discrepancy between the extrapolated precursor-mediated adsorption model reaction probability and the previous stratospheric measurements. The ice surface is in a very dynamic equilibrium at stratospheric conditions with H_2O adsorption and desorption rates of ~ 10−100 ML/s.[24] A variety of experimental studies[41−48] also reveal that a "liquid-like" layer exists on ice over a temperature range from 240 to 273 K. Other theoretical studies and surface

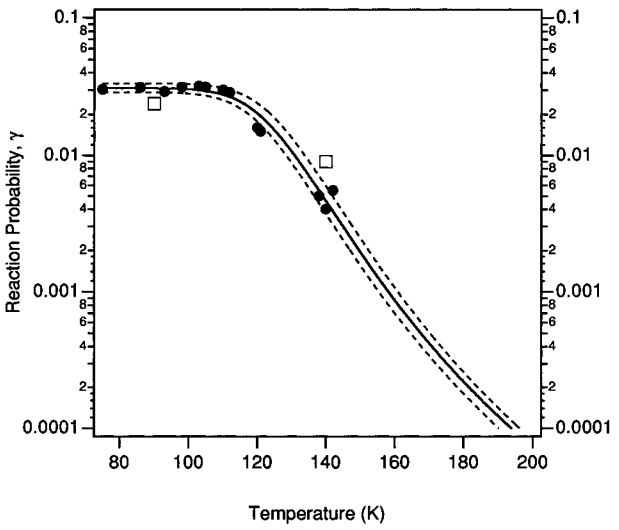

Figure 12. Extrapolation of the reaction probability for $ClONO_2$ hydrolysis on ice from the precursor-mediated adsorption model to stratospheric temperatures. The dashed lines display the possible range of uncertainty.

sensitive low energy electron diffraction (LEED) investigations observe very high amplitude displacements for H_2O molecules on the (001) basal plane of hexagonal ice at temperatures as low as 100 K.[49,50] The $ClONO_2$ hydrolysis reaction probability may be enhanced by the beginnings of a "liquid-like" layer that may exist on the dynamic ice surface under stratospheric temperatures.

The low $ClONO_2$ reaction probability of $\gamma \approx 0.0001$ extrapolated from the precursor-mediated adsorption model could also be the result of high background HNO_3 levels. The $ClONO_2$ hydrolysis reaction probability is extremely sensitive to HNO_3.[7,10] The calibrated HNO_3 LITD signals indicate that the initial ice film has a stoichiometry >25:1 H_2O:HNO_3. This film stoichiometry would lead to an initial HNO_3 surface coverage of ≤ 0.04 ML if the HNO_3 is evenly distributed in the ice film. However, the initial HNO_3 coverage could be ~1 ML if all the HNO_3 is concentrated at the surface. An ice surface partially poisoned by HNO_3 would lead to reaction probabilities somewhere between the reported reaction probabilities of $\gamma \approx 0.3$ on ice and $\gamma \approx 0.001$ on saturated nitric acid-ice surfaces at stratospheric temperatures.[11]

The initial HNO_3 impurity is probably incorporated into the ice film during H_2O deposition. This HNO_3 should be evenly distributed throughout the ice film. In addition, a full monolayer of HNO_3 is produced by the $ClONO_2$ hydrolysis reaction. This measured HNO_3 growth strongly suggests that the initial HNO_3 surface coverage must be low. Consequently, we believe that the surfaces used for these $ClONO_2$ hydrolysis studies should be representative of ice surfaces.

The difference between the $ClONO_2$ reaction probabilities extrapolated from the precursor-mediated adsorption model and the earlier literature values could also be explained by overestimated $ClONO_2$ pressures in the current experiments or inaccurate assumptions regarding the surface area in the previous measurements. The earlier measurements assumed a geometric ice surface area.[51] Consequently, the reported reaction probability may only be an upper limit, and the true reaction probability could be much smaller because of ice film roughness.[8,52,53] Although the $ClONO_2$ reaction probability was relatively independent of ice film thickness,[9] the ice surface roughness may be localized to the near surface region and may not change with film thickness. However, the surface area would need to be higher by almost $\times 1000$ for agreement with the extrapolation from the precursor-mediated adsorption model.

D. Mechanism of $ClONO_2$ Hydrolysis. The temperature-dependent reaction probabilities measured by the LITD studies show that the $ClONO_2$ reaction is efficient even at low temperatures. The precursor-mediated adsorption model yields a reaction barrier of $E_r \sim 3$ kcal/mol. This reaction barrier is consistent with recent ab initio calculations.[21] These calculations show that the lowest energy path for the $ClONO_2$ hydrolysis reaction proceeds through an S_N2 nucleophilic attack by H_2O coupled with proton transfer. The ice lattice plays a key role in the nucleophilic attack. The facile, rapid proton transfer through the ice lattice promotes the formation of hydroxide ions that are much better nucleophiles than H_2O molecules.

The calculations predict that $ClONO_2$ is weakly bound in a reaction complex with $E_d \sim 7$ kcal/mol.[21,38] The reactant configuration is a cyclic ring with one $ClONO_2$ hydrogen-bonded to two H_2O molecules on the ice lattice. Assuming a desorption preexponential of 10^{13} s^{-1}, the $ClONO_2$ in this cyclic ring would have a surface residence time of $\tau_d \sim 8$ s at 110 K and $\tau_d \sim 8$ ms at 140 K. Using the theoretical reaction barrier, $E_r = 3$ kcal/mol, and the reaction preexponential of $\nu_r = 10^6$ s^{-1} from the precursor mediated adsorption model, the reaction lifetimes are $\tau_r \sim 1$ s at 110 K and $\tau_r \sim 50$ ms at 140 K. These lifetimes favor $ClONO_2$ reaction at low temperatures and $ClONO_2$ desorption at high temperatures. These lifetimes will determine the reaction probabilities as predicted by the precursor-mediated adsorption model.

Other laboratory studies suggest that the $ClONO_2$ hydrolysis reaction proceeds through an ionization mechanism.[4,6,22] In one study, the $ClONO_2$ hydrolysis reaction was monitored using Fourier transform reflection absorption infrared spectroscopy (FT-RAIRS).[4] At stratospheric temperatures, the FT-RAIRS spectra was interpreted to reveal that the reactive intermediate [H_2OCl^+] could be isolated under conditions of excess $ClONO_2$. This intermediate was rapidly converted to reaction products upon exposure to additional H_2O. This intermediate suggests that $ClONO_2$ adsorbs and is easily ionized by the ice lattice. The ionized intermediate then proceeds quickly to reaction products.

Recent Knudsen cell experiments support the ionization mechanism.[6] These experiments found that the release of product HOCl was delayed with respect to the $ClONO_2$ exposure. In addition, the reaction did not display mass balance for $ClONO_2$ exposures at 160 K. More Cl was adsorbed onto the ice than was released into the gas phase. This extra Cl was not believed to be HOCl on the ice surface because the extra Cl could not be titrated with HCl. HOCl adsorbed on the ice surface could be titrated with HCl to release Cl_2.[6,9,54,55] Consequently, the HOCl was interpreted as locked up in a "precursor" that is consistent with the [H_2OCl^+] reactive intermediate.[6] We note that this "precursor" is different from the precursor in the precursor-mediated adsorption model.

The "precursor" associated with the [H_2OCl^+] reactive intermediate is formed by the $ClONO_2$ hydrolysis reaction and is believed to delay the release of HOCl.[6] This reactive intermediate has a normal temperature dependence, and more HOCl is produced at higher temperatures.[6] In contrast, the precursor in the precursor-mediated adsorption model is a weakly bound, physisorbed $ClONO_2$ molecule that can either react to form HOCl or desorb prior to reaction. This physisorbed precursor has a negative temperature dependence that yields a decreasing reaction probability with increasing temperature. Both precursors could be present at different stages of the $ClONO_2$ hydrolysis. The physisorbed precursor could

precede the formation of the reactive intermediate "precursor."

The existence of the H_2OCl^+ reactive intermediate suggests that HOCl production should be quenched at the low temperatures used in the LITD studies. The FT-RAIRS studies also report that the $ClONO_2$ hydrolysis reaction is quenched at 80 K.[4] In contrast, the LITD results observe the rapid formation of HOCl at low temperatures and apparently contradict the FT-RAIRS studies. One explanation for this contradiction is that the production of the HOCl LITD signals may be driven by the rapid laser heating. However, this behavior is not expected because many previous studies have shown that laser surface heating with nanosecond lasers promotes desorption over reaction.[40,56,57]

In support of the LITD results and the rapid formation of HOCl in the absence of laser heating, other recent FT-RAIRS studies reveal that the $ClONO_2$ hydrolysis reaction is efficient at low temperatures.[19] Codeposited H_2O and $ClONO_2$ films at 120 K with H_2O:$ClONO_2$ mole ratios greater than 10:1 display FTIR spectra that are consistent with hydrolysis reaction products and no unreacted $ClONO_2$. Molecular $ClONO_2$ peaks could be observed only for very concentrated codeposited films with mole ratios near 1:1 H_2O:$ClONO_2$. Consequently, the earlier codeposited FT-RAIRS film studies[4] may have examined highly concentrated $ClONO_2$ films.

The time delay in the HOCl signal that was observed in the Knudsen cell experiments[6] could also be explained by HOCl stability on ice. Earlier studies observed a delayed release of HOCl that was attributed to HOCl surface stability.[9] The adsorption energy for HOCl on ice has been measured and calculated to be ~14 kcal/mol.[9,58,59] This adsorption energy would lead to HOCl surface lifetimes of 2 days to 20 min at temperatures of 160−180 K, respectively. Consequently, a reactive intermediate is not necessary to explain a delayed HOCl signal that was observed in the recent Knudsen cell experiments.[6]

The lack of Cl mass balance at 160 K observed in these Knudsen cell experiments[6] also does not imply there is a H_2OCl^+ reactive intermediate. The accessibility of the HOCl on ice to titration by HCl may depend on how HOCl is adsorbed on ice. The HOCl and HNO_3 reaction products of the $ClONO_2$ hydrolysis reaction on ice may take up adjacent surface sites. The neighboring HNO_3 and HOCl may slow or prevent HCl from adsorbing or diffusing to an appropriate position for reaction with HOCl. In contrast, HOCl adsorbed directly onto the ice surface would not have to contend with neighboring HNO_3.

V. Conclusions

The reactive uptake of $ClONO_2$ on ice surfaces versus temperature was measured directly in real time with surface sensitivity. The HOCl and HNO_3 hydrolysis products were monitored during $ClONO_2$ exposure using laser-induced thermal desorption (LITD) and mass spectrometric techniques. These studies revealed that $ClONO_2$ hydrolysis on ice is very efficient at temperatures from 75 to 140 K. After longer $ClONO_2$ exposures, the reaction probability decreased as the reaction product coverages reached approximately one monolayer. Calibrated HNO_3 LITD signals revealed that the $ClONO_2$ hydrolysis reaction was strongly inhibited at a HNO_3 coverage of $\sim 7.5 \times 10^{14}$ molecules/cm^2.

A reaction probability of $\gamma = 0.03$ was determined from the time-dependent HOCl and HNO_3 product coverages on the ice surface during $ClONO_2$ exposure. This reaction probability was independent of temperature from 75 to 110 K. The $ClONO_2$ reaction probability decreased with increasing temperature between 110 and 140 K. This decrease was consistent with the temperature-dependent behavior expected from a precursor-mediated adsorption model. Agreement with the precursor-mediated adsorption model indicates that the $ClONO_2$ hydrolysis reaction proceeds with a low activation barrier. The precursor-mediated adsorption model can be extrapolated to stratospheric temperatures to predict a reaction probability. This extrapolation yields a reaction probability of $\gamma = 0.0001$ at 190 K that is much less than earlier experimental measurements of $\gamma = 0.3$. This difference could be caused by the higher pressures and the dynamic ice surface at stratospheric conditions, inaccurate assumptions regarding ice surface area in previous experiments or overestimated $ClONO_2$ pressures and partially HNO_3-poisoned surfaces in the current experiments.

Acknowledgment. This work was supported by grants from NSF (CHE-9528473 and ATM-9321582) and NASA (SASS-94−091). B.S.B. acknowledges support from a NASA GSRP fellowship. M.A.T. was supported as an NSF Young Investigator and a Camille Dreyfus Teacher Scholar. We would like to thank Leah Goldfarb, Steve Barone, and the NOAA Aeronomy laboratory for assistance in synthesizing the $ClONO_2$ and Mark Zondlo for help in storing and handling the $ClONO_2$. We also thank Roberto Bianco for helpful discussions.

References and Notes

(1) Hanson, D. R.; Ravishankara, A. R. *J. Phys. Chem.* **1994**, *98*, 5728.
(2) Hanson, D. R. *J. Phys. Chem.* **1995**, *99*, 13059.
(3) Ravishankara, A. R.; Hanson, D. R. *J. Geophys. Res.* **1996**, *101*, 3885.
(4) Sodeau, J. R.; Horn, A. B.; Banham, S. F.; Koch, T. G. *J. Phys. Chem.* **1995**, *99*, 6258.
(5) Zhang, R.; Leu, M.-T.; Keyser, L. F. *Geophys. Res. Lett.* **1995**, *22*, 1493.
(6) Opplinger, R.; Allanic, A.; Rossi, M. J. *J. Phys Chem. A* **1997**, *101*, 1903.
(7) Chu, L. T.; Leu, M.-T.; Keyser, L. F. *J. Phys. Chem.* **1993**, *97*, 12798.
(8) Leu, M.-T.; Moore, S. B.; Keyser, L. F. *J. Phys. Chem.* **1991**, *95*, 7763.
(9) Hanson, D. R.; Ravishankara, A. R. *J. Phys. Chem.* **1992**, *96*, 2682.
(10) Hanson, D.; Ravishankara, A. R. *J. Geophys. Res.* **1991**, *96*, 5081.
(11) Demore, W. B.; Sander, S. P.; Golden, D. M.; Hampson, R. F.; Kurylo, M. J.; Howard, C. J.; Ravishankara, A. R.; Kolb, C. E.; Molina, M. J. *Jet Propulsion Laboratories Chemical Kinetics and Photochemical Data for use in Stratospheric Modeling*, 1997.
(12) Tolbert, M. A.; Rossi, M. J.; Malhtora, R.; Golden, D. M. *Science* **1987**, *238*, 1258.
(13) Molina, M. J.; Tai-Ly, T.; Molina, L. T.; Wang, F. C.-Y. *Science* **1987**, *238*, 1253.
(14) Wofsy, S. C.; Molina, M. J.; Salawitch, R. J.; Fox, L. E.; McElroy, M. B. *J. Geophys. Res.* **1988**, *93*, 2442.
(15) Nelson, C. M.; Okumura, M. *J. Phys. Chem.* **1992**, *96*, 6112.
(16) Lee, T. J.; Rice, J. E. *J. Phys. Chem.* **1993**, *97*, 6637.
(17) Schindler, T.; Berg, C.; Nieder-Schatteburg, G.; Bondybey, V. *J. Chem. Phys.* **1996**, *104*, 3998.
(18) Abbatt, J. P. D.; Molina, M. J. *J. Phys. Chem.* **1992**, *96*, 7674.
(19) Barone, S.; Zondlo, M.; Tolbert, M. A. *J. Phys. Chem.*, in press.
(20) Hensen, B. F.; Wilson, K. R.; Robinson, J. M. *Geophys. Res. Lett.* **1996**, *23*, 1021.
(21) Bianco, R.; Hynes, J. T. *J. Phys. Chem.*, in press.
(22) Koch, T. G.; Banham, S. F.; Sodeau, J. R.; Horn, A. B.; McCoustra, M. R. S.; Chesters, M. A. *J. Geophys. Res.* **1997**, *102*, 1513.
(23) Berland, B. S.; Haynes, D. R.; Foster, K. L.; Tolbert, M. A.; George, S. M.; Toon, O. B. *J. Phys. Chem.* **1994**, *98*, 4358.
(24) Haynes, D. R.; Tro, N. J.; George, S. M. *J. Phys. Chem.* **1992**, *96*, 8502.
(25) Schmeisser, M. *Inorg. Synth.* **1967**, *9*, 127.
(26) Berland, B. S.; Brown, D. E.; Tolbert, M. A.; George, S. M. *Geophys. Res. Lett.* **1995**, *22*, 3493.
(27) Heavens, O. S. *Optical properties of thin solid films*; Dover Publications: New York, 1991.
(28) We note that there is a sign error on p 80 in Heaven's book, *ibid*. The equation for q_{13} should read $q_{13} = (1 - g_1g_2 + g_2g_3 - g_3g_1) \sin \gamma_1 \cos \gamma_2 + (1 + g_1g_2 - g_2g_3 - g_3g_1) \sin \gamma_2 \cos \gamma_1$.
(29) Maltison, I. H. *J. Opt. Soc. Am.* **1962**, *52*, 1377.

(30) Middlebrook, A. M.; Berland, B. S.; George, S. M.; Tolbert, M. A.; Toon, O. B. *J. Geophys. Res.* **1994**, *99*, 25655.
(31) Arthur, D. A.; Meixner, D. L.; Boudart, M.; George, S. M. *J. Chem. Phys.* **1991**, *95*, 8521.
(32) Foster, K. L.; Tolbert, M. A.; George, S. M. *J. Phys Chem. A* **1997**, *101*, 4979.
(33) Stern, S. A.; Mullhaupt, J. T.; Kay, W. B. *Chem. Rev. (Washington, D.C.)* **1960**, *60*, 185.
(34) Pruppacher, H. R.; Klett, J. D. *Microphysics of clouds and precipitation*; D. Reidel Publishing Co.: Dordrecht, Holland, 1980.
(35) Winkler, A.; Rendulic, K. D.; Wendl, K. *Appl. Surf. Sci.* **1982**, *14*, 209.
(36) Weinberg, W. H. Kinetics of Interface Reactions. In *Dynamics of Gas-Surface Reactions*; Rettner, C. T., Ashfold, M. N. R., Eds.; Royal Society of Chemistry: Cambridge, 1991.
(37) King, D. A.; Wells, M. G. *Proc. R. Soc. London A* **1974**, *339*, 245.
(38) Bianco, R.; Hynes, J. T. Personal communication, 1997.
(39) Tabazadeh, A.; Turco, R. P.; Drdla, K.; Jacobson, M. Z.; Toon, O. B. *Geophys. Res. Lett.* **1994**, *21*, 1619.
(40) Deckert, A. A.; Brand, J. L.; Mak, C. H.; Koehler, B. G.; George, S. M. *J. Chem. Phys.* **1987**, *87*, 1936.
(41) Jellinek, H. H. G. *J. Colloid Interface Sci.* **1967**, *25*, 192.
(42) Golecki, I.; Jaccard, C. *J. Phys. C: Solid State Phys.* **1978**, *11*, 4229.
(43) Beaglehole, D.; Nason, D. *Surf. Sci.* **1980**, *96*, 357.
(44) Gilpin, R. R. *J. Colloid Interface Sci.* **1980**, *77*, 435.
(45) Furukawa, Y.; Yamamoto, M.; Kuroda, T. *J. Cryst. Growth* **1987**, *129*, 665.
(46) Elbaum, M.; Lipson, S. G.; Dash, J. G. *J. Cryst. Growth* **1993**, *129*, 491.
(47) Dosch, H.; Lied, A.; Bilgram, J. H. *Surf. Sci.* **1995**, *327*, 145.
(48) Mizuno, Y.; Hanfusa, N. *J. Phys. Collog.***1987**, *48*, C1.
(49) Materer, N.; Starke, U.; Barbieri, A.; Van Hove, M. A.; Somarjai, G. A.; Kroes, G.-J.; Minot, C. *J. Phys. Chem.* **1995**, *99*, 6267.
(50) Materer, N.; Starke, U.; Barbieri, A.; Van Hove, M. A.; Somorjai, G. A.; Kroes, G.-J.; Minot, C. *Surf. Sci.* **1997**, *381*, 190.
(51) Hanson, D. R.; Ravishankara, A. R. *J. Phys. Chem.* **1993**, *97*, 2802.
(52) Keyser, L.; Leu, M.-T. *J. Colloid Interface Sci.* **1993**, *155*, 137.
(53) Keyser, L. F.; Leu, M.-T. *Micros. Res. Technol.* **1993**, *25*, 434.
(54) Zhang, R.; Jayne, J. T.; Molina, M. J. *J. Phys. Chem.* **1994**, *98*, 867.
(55) Abbatt, J. P. D.; Molina, M. J. *Geophys. Res. Lett.* **1992**, *19*, 461.
(56) Deckert, A. A.; George, S. M. *Surf. Sci.* **1987**, *182*, L215.
(57) Hall, R. B. *J. Phys. Chem.* **1987**, *91*, 1007.
(58) Turco, R. P.; Toon, O. B.; Hamill, P. *J. Geophys. Res.* **1989**, *94*, 16493.
(59) Brown, A. R.; Doren, D. J. *J. Phys. Chem. B* **1997**, *101*, 6308.